Journal of Physics and Chemistry of Solids 135 (2019) 109076

Contents lists available at ScienceDirect

Journal of Physics and Chemistry of Solids

journal homepage: www.elsevier.com/locate/jpcs

Magnetoelectric and HR-STEM investigations on eutectic $CoFe_2O_4$–$Ba_{1-x}Sr_xTiO_3$ composites

Martin Breitenbach[a], Hakan Deniz[b], Stefan G. Ebbinghaus[a,*]

[a] Martin-Luther-Universität Halle-Wittenberg, Institut für Chemie, Kurt-Mothes-Straße 2, D-06120, Halle/Saale, Germany
[b] Max-Planck-Institut für Mikrostrukturphysik, Weinberg 2, D-06120, Halle/Saale, Germany

ARTICLE INFO

Keywords:
Composite materials
Interfaces
Crystal growth
Electron microscopy
Magnetoelectric properties

ABSTRACT

Multiferroic $Ba_{1-x}Sr_xTiO_3$–$CoFe_2O_4$ (x = 0.03, 0.05) composites with rarely investigated 3-3 connectivity were prepared by eutectic crystallization in an optical floating zone furnace. High-resolution scanning transmission electron microscopy investigations of the $CoFe_2O_4$–$BaTiO_3$ interface revealed an almost perfect connection between both components. These micrographs also showed that the impact of post-annealing in air was much larger than expected and resulted in formation of small $BaTiO_3$ inclusions in the $CoFe_2O_4$ phase. The magnetoelectric coefficient α_{ME} was studied in detail with respect to its dependence on the static magnetic field, the frequency of the driving AC-field and temperature. Furthermore, the influence of different growth rates (5, 10 and 20 mm h^{-1}), chemical composition, sample thickness and the alignment of electrical polarization and magnetic field (collinear or vertical) on the magnetoelectric properties were studied. The largest value of α_{ME} = 1.3 mV Oe^{-1} cm^{-1} was found for a sample grown at 5 mm h^{-1}. For even slower growth rates, a higher Sr content was required to avoid the formation of impurity phases leading to a decrease of α_{ME}.

1. Introduction

Materials that combine at least two ferroic orderings are called multiferroics. The interaction of these ferroic ordering phenomena leads to a variety of novel applications such as new memory devices, sensors or spintronics [1,2]. The so-called magnetoelectric (ME) effect, first verified experimentally by Astrov in 1960 [3], results from a coupling of ferroelectricity with ferro- or ferri-magnetism. The ME effect allows changing the magnetization by applying an electric field (converse ME effect) [4,5], or modifying the electrical polarization by a magnetic field (direct ME effect) [2–4,6]. There are numerous single-phase ME materials like $BiMnO_3$ [7] but for most of them the ME effect is rather small and/or occurs only at low temperatures. Therefore, multi-component multiferroics have received increasing interest because many show strong and stable ME coupling even above room temperature [8–10]. Such magnetoelectric composites usually contain a piezoelectric (and ferroelectric) compound like $PbZr_xTi_{(1-x)}O_3$ [8,9] or $BaTiO_3$ [11–13] and a magnetostrictive (and ferro-/ferri-magnetic) material like $CoFe_2O_4$ [9,14,15] or $NiFe_2O_4$ [12,16,17]. In composites, electric and magnetic order have different origins, and so can be classified as type-I multiferroics [18]. In addition to the choice of components, the ME properties also depend on synthesis methods, particle morphology, quality of the interface and connectivity (e.g. 0–3, 2-2 or 1–3), providing additional opportunities for optimization.

In particular, there are many studies on the $BaTiO_3$–$CoFe_2O_4$ system prepared by a wide variety of methods like solid-state synthesis [15], polyol-mediated synthesis [13], spin coating [14,19], pulsed laser deposition (PLD) [20] and template-mediated methods [21]. In this work, we apply a rarely used method – crystallization of an eutectic melt in an optical floating zone furnace as recently described in detail [22]. First experiments on such eutectics by Van den Boomgaard et al. [23,24] in the early 1970s revealed the formation of very interesting geometric structures and a high ME effect; however, the samples contained relatively large amounts of $BaFe_{12}O_{19}$ as impurity. Surprisingly, the approach of eutectic crystallization was not further investigated (possibly due to high cost), until in 2000 when Echigoya et al. [25] studied the influence of growth rate, composition and atmosphere during the solidification process of $BaTiO_3$–$CoFe_2O_4$. Unfortunately, they did not present any ME investigations.

We previously reported successful growth of phase-pure $BaTiO_3$–$CoFe_2O_4$ composites in pure nitrogen [22]. An oxygen-free atmosphere was essential to avoid formation of $BaFe_{12}O_{19}$. Another crucial step was a small Sr substitution (3 mol%), which prevented formation of the non-ferroelectric hexagonal $BaTiO_3$ modification. Due

* Corresponding author. Martin-Luther-Universität Halle-Wittenberg, Institut für Chemie, Kurt-Mothes-Straße 2, D-06120, Halle/Saale, Germany
E-mail addresses: martin.breitenbach@chemie.uni-halle.de (M. Breitenbach), hakan.deniz@mpi-halle.mpg.de (H. Deniz), stefan.ebbinghaus@chemie.uni-halle.de (S.G. Ebbinghaus).

https://doi.org/10.1016/j.jpcs.2019.109076
Received 27 August 2018; Received in revised form 18 June 2019; Accepted 19 June 2019
Available online 23 June 2019

to the non-oxidizing atmosphere, the as-grown samples were electrically conductive. Thus reoxidation in air was necessary to heal the oxygen defects, resulting in a very strong enhancement of the resistance (> 20 MΩ). After electric polarization, first measurements revealed promising ME properties.

The aim of the present study therefore is the detailed characterization of the ME coefficients of the samples with respect to the influence of the static magnetic field (H_{dc}), the frequency of a superimposed alternating magnetic field (H_{ac} = 10 Oe) and temperature. It turns out that α_{ME} increases for samples crystallized with slower growth rates but decreases for Sr substitutions exceeding 3 mol%. Another remarkable result is the increase of α_{ME} when the sample thickness is reduced and an opposite sign of α_{ME} when the magnetic field is aligned perpendicular to the polarization.

2. Experimental

2.1. Preparation

We used $BaCO_3$ (≥99%, Solvay), TiO_2 (≥99%, Sachtleben) and $SrCO_3$ (≥99%, Merck) to prepare Sr-doped $BaTiO_3$ with 1 mol% Ti-excess. $CoFe_2O_4$ was prepared from stoichiometric amounts of Co_3O_4 (≥99.7%, Alfa Aesar) and Fe_2O_3 (≥99%, Sigma-Aldrich). Reactions were performed in air for 2 h at 1373 K. The obtained powders were mixed in the molar ratio 0.38 $CoFe_2O_4$/0.62 $Ba_{(1-x)}Sr_xTiO_3$ and hydrostatically pressed to rods at 70 MPa, which were sintered at 1473 K for 10 h. Further details are given in our previous study [22].

The rods consisting of the eutectic composition for the system (38 mol% $CoFe_2O_4$/62 mol% $BaTiO_3$) [23,25] were molten/crystallized in a four-mirror floating zone furnace (CSC FZ-T-10000-H-HR-I-VPO-PC) equipped with 1500 halogen lamps under flowing pure nitrogen (5 N purity, gas flow 12 L h^{-1}) with seed and feed counter-rotating at 20 rpm. Different growth rates in the range of 2.5–20 mm h^{-1} were used. See our previous study for further experimental details [22]. The obtained crystal boules were cut into slices of 0.7 mm thickness perpendicular to the growth direction and were reoxidized in static air for 10 h at 973 K (heating rate 5 K min^{-1}). These reoxidized slices were used for subsequent X-ray diffraction (XRD) measurements and detailed ME characterization.

2.2. Characterization

A Bruker D8 Advance diffractometer operating in Bragg–Brentano geometry with Cu-Kα radiation and equipped with a one-dimensional silicon strip detector (LynxEye™) was used for powder XRD measurements (angular range 15–75°2θ, step size 0.01°2θ and counting rate 1 s per data point). Scanning electron microscopy (backscattered electron mode) was performed on the polished samples (Struers LaboPol-5, grinding: SiC paper grit 1200, 2000; polishing: diamond suspension 2–6 μm) in a Phenom ProX with an acceleration voltage of 15 kV. For transmission electron microscopy investigation of the $BaTiO_3$–$CoFe_2O_4$ interface electron-transparent lamellae in cross-section geometry from each sample were prepared by a FEI Nova 600 Nanolab focused ion beam (FIB) system. For each sample, two lamellae were cut in close proximity from an interface between grains having 90° edges with each other. These lamellae were cleaned with O_2 plasma to prevent carbon contamination during imaging. Scanning transmission electron microscopy (STEM) study of the lamellae was performed using a probe-corrected FEI TITAN 80–300 microscope operated at 300 kV, equipped with a high-angle annular dark-field detector for Z-contrast imaging and a Si(Li) detector for energy dispersive X-ray (EDX) spectroscopy. The FEI TIA software was used for analysis and processing of EDX measurements.

Single crystal XRD was carried out on a STOE IPDS-2T imaging plate diffractometer operating with Mo-K_α radiation. In total, 360 frames were recorded with an irradiation time of 2 min $frame^{-1}$ in the ω-range of 0–180° with Δω = 1° for φ = 0° and 90°, respectively. The detector distance was set to 60 mm, resulting in $2\theta_{max}$ = 70°.

For electrical contacts, both sides of the reoxidized slices were sputtered with gold electrodes of 100 nm thickness in a Cressington 108 auto sputter coater. The polarization of $BaTiO_3$ was accomplished by applying an electric field of 5 kV cm^{-1} (current limit: 0.1 mA) for 12 h. Afterwards, the contacts were short-circuited for 5 min. In contrast to our earlier experiments [22], the poling procedure was carried out at room temperature.

The ME measurements were performed in a Quantum Design Physical Property Measurement System PPMS-9 using a self-made setup as previously described [13]. The magnetic DC-field was varied in the range −10 to 10 kOe. A small collinear alternating magnetic field of H_{ac} = 10 Oe with frequencies of 100–1000 Hz was superimposed by a solenoid. Frequency-dependent ME measurements at 300 K in the range 50–1000 Hz with 3-Hz steps were carried out in the magnetic DC-field at which the maximum α_{ME} value was found (ca. 2000 kOe). Finally, the temperature dependence of the ME effect was measured for 10–300 K with 2-K steps again in the magnetic DC-field corresponding to α_{ME}(max). For calculation of the ME coefficient, the real part (in-phase contribution) of the measured AC-voltage was divided by the AC-field (H_{ac}) and sample thickness (d):

$$\alpha_{ME} = \frac{U_{ac}}{H_{ac} \cdot d} \quad (1)$$

3. Results and discussion

3.1. SEM, high-resolution (HR)-STEM and single crystal XRD investigations

From composite boules grown at 5, 10 and 20 mm h^{-1}, slices were cut, polished and reoxidized as described in the experimental section. A SEM micrograph of one representative slice is shown in Fig. 1.

By self-organization during the eutectic crystallization, a variety of different randomly distributed geometric structures are formed. As described previously in more detail [22], these structures can be roughly divided into regions of rather globular particles embedded in a matrix and regions in which $CoFe_2O_4$ and $BaTiO_3$ form an intergrowth with a very regular geometric arrangement and long linear interfaces. These structures can be of very different sizes (Fig. 1). The same type of entanglement is found perpendicular and parallel to the growth direction. Thus, the two phases form a three-dimensional interpenetrating network that can best be classified as 3-3 connectivity. This type of microstructure – also denoted as “Chinese script” – is frequently observed in directionally solidified eutectic oxides [26].

For a more detailed characterization of the $CoFe_2O_4$–$BaTiO_3$ interfaces, high-resolution STEM investigations were carried out on an as-grown and a reoxidized slice of the sample grown at 5 mm h^{-1}. These

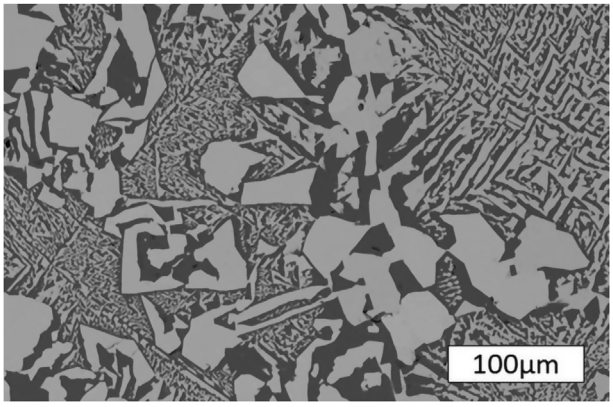

Fig. 1. SEM image (BSE mode) of a crystal slice cut from the sample grown at 10 mm h^{-1}.

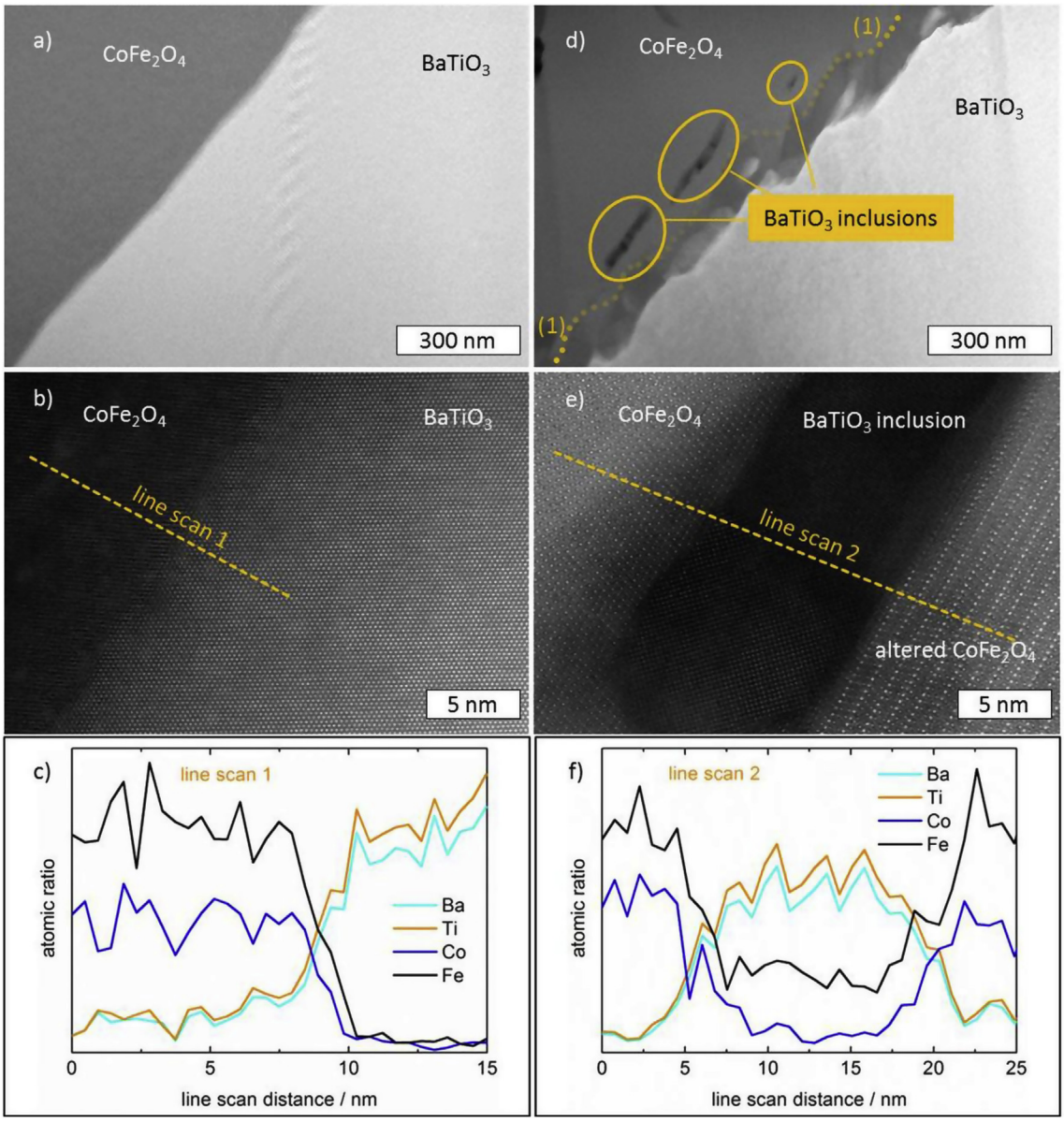

Fig. 2. HR-STEM images showing an overview (top), a detailed view (middle) of the $CoFe_2O_4$–$BaTiO_3$ interface and an EDX line scan (bottom) in the as-grown (left) and a reoxidized (right) sample crystallized at 5 mm h^{-1}.

HR-STEM images are displayed in comparison for two different magnifications in Fig. 2.

The two different phases in the as-grown samples (Fig. 2a and b) were identified as $CoFe_2O_4$ (dark) and $BaTiO_3$ (bright) from the d-spacings (data not shown) and an EDX line scan (line scan 1). The images reveal the close connection of $CoFe_2O_4$ and $BaTiO_3$, i.e. the interfaces show no pinholes or voids. A further image analysis reveals (tilted) epitaxy between $CoFe_2O_4$ (CFO) and $BaTiO_3$ (BTO). Fig. S1b depicts a fast Fourier transform (FFT) pattern from the full image area of Fig. 2b. As seen in this FFT pattern, the (111) BTO and (311) CFO reflections appear very close to each other in the reciprocal space. A filtered image obtained using only these reflections shows that the lattice planes of both phases align with a slight tilt angle (Fig. S1c).

Large differences between the as-grown and the reoxidized samples can be seen in the overview graph (Fig. 2d). Upon reoxidation, the interface becomes more irregular and orientation of the ferrite close to it changes (indicated with a yellow dotted line (1)). Additionally, dark inclusions occur near the interface inside the $CoFe_2O_4$ regions, whereas no changes are found inside the $BaTiO_3$ areas. These dark inclusions are identified as (Fe-substituted) $BaTiO_3$ by an EDX line scan (line scan 2). The inclusions appear much darker than the main $BaTiO_3$ area. This might be due to their different orientation and in turn a much higher orientation contrast or to a deviating sample thickness at this spot resulting from the FIB preparation. Another reason might be a strain contrast because the BTO is located inside the CFO matrix, which possesses a large lattice mismatch. The higher magnification (Fig. 2e) reveals no epitaxial relationship between the inclusions and the surrounding $CoFe_2O_4$ matrix. In addition, the ferrite between the inclusions and the interface to the main $BaTiO_3$ region possesses a different orientation compared to the inner part of the $CoFe_2O_4$ grain. Although the EDX line scan provides no clear hints for chemical reactions at the BTO–CFO interface, we cannot rule out an interdiffusion of cations as, for example, observed by Tileli et al. in PLD films [27]; however, formation of a hexaferrite phase or an ilmenite-type phase as proposed by these authors seems unlikely. In the right region of Fig. 2e (denoted as altered $CoFe_2O_4$), lattice parameters of 9.93 and 4.34 Å were measured. These do not match with the ilmenite-type phase or with $BaFe_{12-2x}Co_xTi_xO_{12}$. The closest possible match is $Ba_{11}Fe_8Ti_9O_{41}$

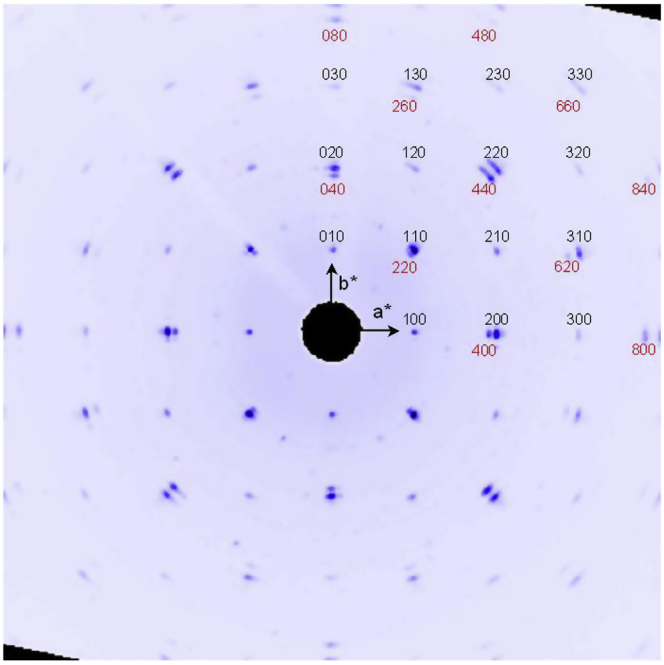

Fig. 3. The hk0-plane of the reciprocal lattice in the range $-1\,Å^{-1}$ to $+1\,Å^{-1}$ (reconstructed from 360 XRD imaging plates) of a $BaTiO_3$–$CoFe_2O_4$ crystal (approximately 200 µm diameter) grown at 20 mm h^{-1}.

($d_{(107)}$ = 4.33 Å, $d_{(006)}$ = 10.24 Å). The EDX line scan confirms the presence of Co in this region and so formation of this phase also seems unlikely.

The STEM results reveal that the reoxidation process has a much stronger impact on the composites than just the healing of oxygen defects. It would therefore be interesting to study its influence on the ME properties. Unfortunately, this was not possible because α_{ME} cannot be measured on the as-grown samples due to their high electrical conductivities.

TEM is a local technique providing information only for a very small section of the sample. We therefore used single crystal XRD as a complementary, global method. Cube-shaped samples with approximately 200 × 200 × 200 µm were cut from different crystal bowls and measured on an imaging plate diffractometer as described in the experimental section. From the 360 frames recorded, the reciprocal lattice was reconstructed using STOE X-area software. As a representative example, Fig. 3 shows the hk0-plane in the range $-1\,Å^{-1} \leq a^* \leq +1\,Å^{-1}$, $-1\,Å^{-1} \leq b^* \leq +1\,Å^{-1}$ of a crystal grown at 20 mm h^{-1}. Reciprocal lattice points with $h,k \geq 0$ of BTO and CFO are labeled in black and red, respectively. The sample possesses a high mosaicity as reflected, for example, by elongation of the 220_{BTO} peak and consists of at least two domains leading to additional intensities visible e.g. in the vicinity of the 110_{BTO} peak and its equivalents. On the other hand, the presence of well-defined reciprocal lattice points clearly proves the crystalline character of the eutectic composite. Contributions of the two components BTO and CFO can easily be distinguished from their deviating d* values corresponding to $a_{BTO} \approx 4.00$ Å and $a_{CFO} \approx 8.40$ Å, respectively, in good agreement with powder XRD results [22]. For $CoFe_2O_4$, the systematic reflection conditions 0*k*0: $k = 4n$, *h*00: $h = 4n$ and *hk*0: $h + k = 4$, $h = 2n$, $k = 2n$ are obviously fulfilled. The seemingly missing 660-reflection has too low an intensity to be visible ($I_{rel} < 1\%$).

Remarkably, the arrangement of reciprocal lattice points clearly shows an epitaxial relationship of the two phases, i.e. BTO(001)[100]||CFO(001)[100] in accordance with the electron diffraction results of Echigoya et al. [25]. However, because of the slightly diffuse character of the spots, small angle tilts between BTO and CFO cannot be ruled out. We emphasize that, in contrast to electron diffraction, XRD integrates over the entire sample (i.e. a cube with approximately 200 µm edge length) thus providing global information on the epitaxy.

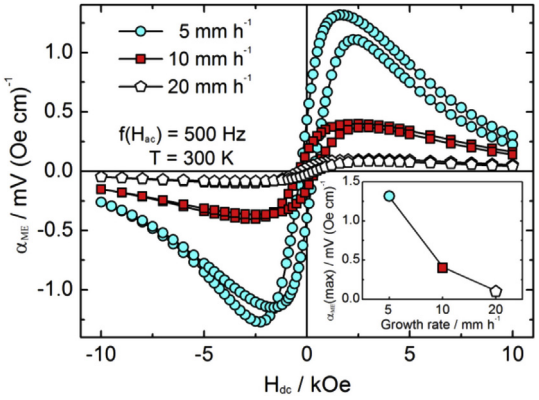

Fig. 4. DC-field dependent ME coefficients of samples grown at different crystallization rates.

3.2. DC-field dependence of $\alpha_{(ME)}$

Prior to the investigations, sample slices with 0.7 mm thickness were electrically polarized as described in the experimental section. Unfortunately, we were unable to measure conclusive P(E)-curves because the samples were still too conductive. We therefore cannot prove that saturation polarization is achieved. However, a successful (partial) polarization is evident by two experimental observations: first no ME effect is detected without the poling step and second the sign of α_{ME} is inverted when a reverse electrical field is applied (Fig. S2).

The ME measurements were carried out at 300 K with f (H_{ac}) = 500 Hz. Starting from H_{dc} = 10 kOe the magnetic field was decreased to −10 kOe and re-increased to 10 kOe. The results are displayed in Fig. 4.

The ME effect increases significantly with slower crystallization speeds. As previously shown [22], the samples show densities in the range 94–98% of their fraction-weighted crystallographic values regardless of growth speed. In addition, sizes of the geometric structures do not change significantly for the three samples. Thus, although sample density and the size of the interface area between $CoFe_2O_4$ and $BaTiO_3$ does not change significantly, slower crystallization leads to stronger ME coupling.

We emphasize that crystallization speed has no significant impact on the magnetic properties of the samples. The saturation magnetization of all samples is almost identical and close to the theoretical value of 3 μ_B f.u.$^{-1}$ expected for $CoFe_2O_4$ (Fig. S3). In addition, remanent magnetizations and coercitivities are also very similar.

The DC-field at which the ME coefficients reach their local maximum and minimum (denoted as H_{dc}(max) and H_{dc}(min)) largely depends on the sweep direction for all samples. Upon decreasing the DC-field from 10 to −10 kOe, the maximum α_{ME} values occur for H_{dc}(max) of 1.6–2.0 kOe and the minimum for H_{dc}(min) of −2.0 to −2.6 kOe. When the field is re-increased, the values for H_{dc}(min) and H_{dc}(max) exchange. This shift of α_{ME}(max) was also observed in our earlier experiments [22] and for $BaTiO_3$–$CoFe_2O_4$ bulk composites [28,29]. The growth rate in the floating zone process has a small effect on the shape of the ME curve but a large impact on absolute values of α_{ME}. Its maximum values are shown in the inset of Fig. 4 and represent α_{ME}(max) = 1.3, 0.4 and 0.1 mV Oe^{-1} cm^{-1} for samples grown at 5, 10 and 20 mm h^{-1}, respectively. Thus one might expect even larger ME values for slower growth rates. Unfortunately, this is not the case due to issues discussed below.

It is furthermore striking that during the re-increasing of the magnetic field, slightly smaller α_{ME} values are found than during the initial

sweeps. This effect is due to a slowly fading polarization of the ferroelectric component. Upon repetition of the poling procedure this fatigue effect vanishes.

Our ME results can be compared to values reported in the early work of Van den Boomgaard et al. [23,24]. Although a different sample geometry (length 45 mm, diameter 4.5 mm) was used and measurements were carried out under resonance conditions at ~60–70 kHz, the reported values of 1–4 mV cm^{-1} Oe^{-1} are comparable to our results. Only for one sample with a strongly deviating chemical composition, a much larger value of 50 mV cm^{-1} Oe^{-1} could be achieved. We note that the reported composition [23,24] is far from that calculated for the eutectic $(BaTiO_3)_{0.62}(CoFe_2O_4)_{0.38}$. In fact, the authors admit that "there are some indications that it [the magneto plumbite phase $BaFe_{12-2x}Co_xTi_xO_{19}$] plays a role in the composite materials with the greatest magnetoelectric effect" and "Microprobe analysis revealed that a part of the coarse precipitates in the cell walls consisted of the M [magneto plumbite] phase" [23]. Furthermore, the authors pointed out that their spinel phase was not pure $CoFe_2O_4$ but $CoFe_{2-2x}Co_xTi_xO_4$. In a later article, Van den Boomgaard reported that the material in fact consisted of $BaTiO_3$, $CoFe_{2-x}Ti_xCo_xO_4$ and $BaFe_{12-2y}Co_yTi_yO_{19}$ [30]. We therefore conclude that the large ME values observed by Van den Boomgaard and Van Run were not the intrinsic values of the $BaTiO_3/CoFe_2O_4$ system but resulted from the contribution of barium hexaferrite at the interface plus the deviating composition of the spinel phase. In this context we emphasize that the chemical composition of our samples corresponds to the nominal one of the eutectic, with no hints of secondary phases in either the XRD or TEM investigations.

3.3. AC-frequency dependence of $\alpha_{(ME)}$

The sample grown at 5 mm h^{-1} was used to investigate α_{ME} with different AC-field frequencies (Fig. 5).

For f(H_{ac}) = 100 Hz, the lowest ME coefficients were measured. The values increase with frequencies up to 500 Hz. For even higher frequencies, nearly identical values are found, almost twice those for 100 Hz. Apart from this, the other curve characteristics like coercitivity of H_{dc} (300 Oe), the position of the local ME maxima (± 1.6 and ± 2.2 kOe) and their dependence on the sweep direction are nearly identical for all frequencies.

Frequency dependence of α_{ME} for the three samples grown at 5, 10 and 20 mm h^{-1} are shown in Fig. 6. Measurements were carried out at 300 K and H_{dc} = 2000 Oe, i.e. close to the maximum ME effect.

All samples show a similar behavior except for the absolute values of $\alpha_{(ME)}$. At low frequencies, the ME coefficients increase with f(H_{ac}) and saturate in the region 300–400 Hz. At higher frequencies, nearly constant values occur. For composites grown at 10 and 20 mm h^{-1}, values of 0.4 and 0.1 mV Oe^{-1} correspond to their maximum values

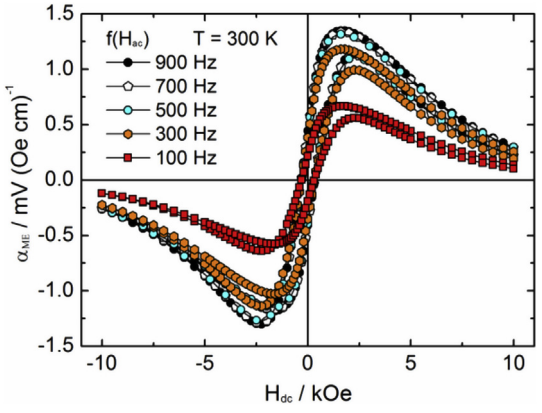

Fig. 5. DC-field dependent ME coefficient of the sample grown at 5 mm h^{-1} measured at different frequencies of the superimposed AC-field.

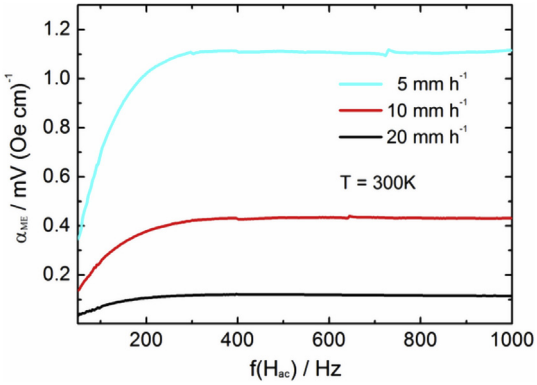

Fig. 6. AC-frequency dependence of the ME coefficent.

shown in Fig. 4. The ME coefficient α_{ME} = 1.1 mV Oe^{-1} cm^{-1} for the 5 mm h^{-1} sample is a little lower than its maximum (α_{ME} = 1.3 mV Oe^{-1} cm^{-1}, Fig. 4). This can be explained by a slight difference between the applied DC-field of H_{dc} = 2000 Oe and the exact H_{dc} of 1600 Oe for α_{ME}(max).

We did not detect resonance conditions in the investigated frequency range. This is not surprising, because such resonances typically occur in a range of 15–430 kHz [31,32], which unfortunately cannot be accessed with our setup. The visible small jumps (Fig. 6) are not reproducible and are probably due to electrical glitches.

The frequency dependency of the samples grown by floating zone melting is similar to our earlier investigations on 0–3 composites of the $CoFe_2O_4$–$BaTiO_3$ system [13]. This indicates that the frequency-dependent ME properties mostly depend on the composite system and not on its connectivity or the synthesis route.

3.4. Temperature dependence of $\alpha_{(ME)}$

A static magnetic field of H_{dc} = 2000 Oe and a frequency of f(H_{ac}) = 500 Hz was used for measurements of the temperature dependence of α_{ME} (Fig. 7).

For all three growth rates, the ME coefficients at room temperature are in accordance with the corresponding values from the DC field- and AC frequency-dependent measurements. With decreasing temperatures, α_{ME} increases until a maximum at 260–270 K. At lower temperatures, the ME coefficient again decreases and becomes undetectably small below 160 and 120 K for samples grown at 20 and 10 mm h^{-1}, respectively. In contrast, for the sample grown at 5 mm h^{-1}, measurable α_{ME} values occur down to 10 K.

The maximum values of α_{ME} are found in the temperature region of the orthorhombic–tetragonal phase transition of $BaTiO_3$. For pure $BaTiO_3$, the transition temperature has been reported to be within 265–280 K but is known to depend both on the crystallite sizes and on

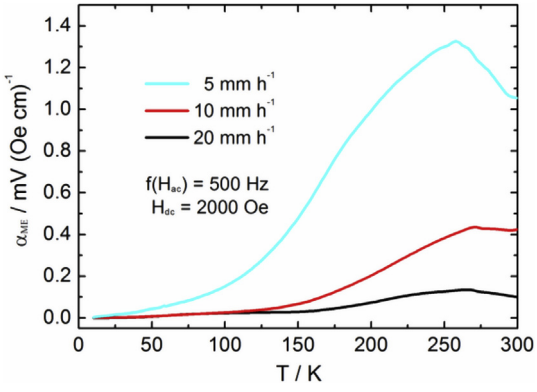

Fig. 7. Temperature dependence of the ME coefficient.

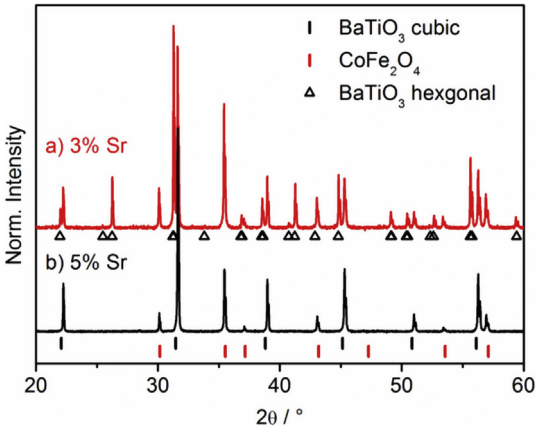

Fig. 8. XRD patterns of composites grown at 2.5 mm h^{-1}.

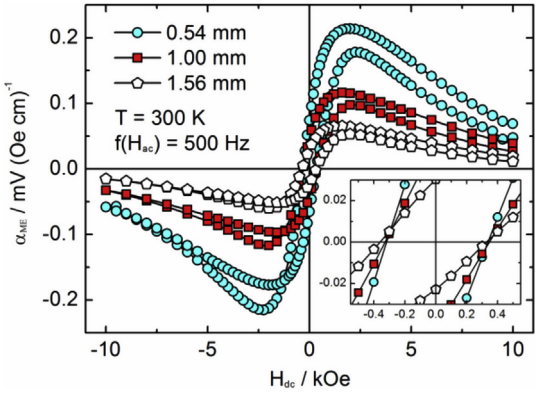

Fig. 9. Field-dependent ME coefficients of the composite $(CoFe_2O_4)_{0.38}$–$(Ba_{0.95}Sr_{0.05}TiO_3)_{0.62}$ grown at 2.5 mm h^{-1} for three different sample thicknesses.

substitutions. In particular, Sr substitution shifts the transition to lower temperatures [33]. Such substitution effects may also explain why the sample grown at 5 mm h^{-1} has its ME maximum at a slightly lower temperature than the others – a slower growth rate leads to trace incorporations of Fe in $BaTiO_3$, which is known to lower the orthorhombic–tetragonal phase transition temperature [34].

The observed temperature dependence of α_{ME} can be understood taking into account that the ME effect is generally accepted to be a product property of the magnetostriction of $CoFe_2O_4$ and the piezoelectricity of $BaTiO_3$, which changes upon the tetragonal–orthorhombic phase transition [35].

3.5. Influence of growth rate and Sr content on phase composition and $\alpha_{(ME)}$

The above-mentioned results show that slower growth rates result in larger ME responses. Therefore, an additional sample was crystallized at 2.5 mm h^{-1}. This decreased speed has a strong impact on the composition. The XRD measurements reveal large amounts of the undesired non-ferroelectric hexagonal modification of $BaTiO_3$ (Fig. 8a). Because Sr doping effectively suppresses the formation of hexagonal barium titanate [36], we raised the Sr content from 3 to 5 mol% in a subsequent floating zone experiment.

The composite with the larger Sr content (Fig. 8b) consists only of $CoFe_2O_4$ and $BaTiO_3$ without detectable reflexes of the hexagonal modification. Rietveld refinement measurements revealed slightly smaller lattice parameters for $Ba_{0.95}Sr_{0.05}TiO_3$ before reoxidation ($a_{as\text{-}grown}$ = 4.0048 Å, $c_{as\text{-}grown}$ = 4.0075 Å) and after reoxidation (a_{reox} = 4.0019 Å, c_{reox} = 4.0044 Å) compared to corresponding values for $Ba_{0.97}Sr_{0.03}TiO_3$ of ($a_{as\text{-}grown}$ = 4.0066 Å, $c_{as\text{-}grown}$ = 4.0093 Å, a_{reox} = 4.0043 Å, c_{reox} = 4.0077 Å) [21], reflecting the smaller ionic radius of Sr^{2+} (1.44 Å) compared to Ba^{2+} (1.61 Å) [37]. Apparently, slower growth rates promote the formation of hexagonal $BaTiO_3$, which can be suppressed by higher amounts of Sr. We note that the tetragonal distortion of both samples (i.e. with 3 and 5 mol%) is very small. Consequently, the XRD pattern can as well be fitted using the cubic perovskite structure. Even so, we chose the tetragonal $BaTiO_3$ modification as the ME measurements clearly indicate the presence of ferroelectricity.

The sample containing $Ba_{0.97}Sr_{0.03}TiO_3$ grown at 2.5 mm h^{-1} (i.e. the one containing hexagonal $BaTiO_3$) shows no measurable the ME effect. In contrast, the sample with 5 mol% Sr shows a pronounced ME signal. From this crystal, slices of different thicknesses were cut to investigate the influence of the sample thickness on α_{ME} (Fig. 9).

First, it is striking that the ME coefficients are far smaller compared to the sample substituted with 3 mol% Sr and grown at 5 mm h^{-1}. This finding shows that the (possible) benefits of a slower growth rate are clearly overcompensated by the negative effects of the larger Sr content. The reduction of α_{ME} due to Sr substitution is caused by the lower polarization, which was reported to change from 20 μC cm^{-2} for pure $BaTiO_3$ to 8 μC cm^{-2} for $Ba_{0.95}Sr_{0.05}TiO_3$ [38,39] and is also reflected in the decrease of tetragonal distortion (c/a ratio). For x = 0.03, there is a value of c/a = 1.0008 in our reoxidized samples, which changes to c/a = 1.0006 for x = 0.05.

To obtain high ME coefficients for floating zone-grown composites it is therefore necessary to find a compromise between a slow growth rate (which enhances α_{ME} but increases the risk of forming hexagonal $BaTiO_3$) and the Sr content (which acts in the reverse way). It should be noted that the sample with 5 mol% Sr also shows the shift of H_{dc}(max).

The pronounced differences in the ME values for the three samples thicknesses (0.5, 1.0 and 1.5 mm) are quite unexpected since this value is taken into account in calculation of the ME coefficients (Eq. (1)). It should be noted that the measured slices are cut from the same region of one crystal boule. In fact, only the absolute values of α_{ME} differ while all other parameters such as the general course of curves, location of α_{ME}(max) or coercitivities are basically identical. One explanation for the decrease of α_{ME} with sample thickness is increasing electric losses (leakage currents) within the samples due to their finite conductivity.

To measure the transverse ME effect, slices were turned by 90°. In this orientation the ferroelectric polarization is aligned perpendicular to H_{dc} and H_{ac} instead of the usual collinear alignment (Fig. 10). Comparison of ME measurements in longitudinal and transverse alignment is shown in Fig. 11.

Upon turning the samples by 90° the ME effect changes its sign. The absolute α_{ME} values in vertical alignment are about 30% smaller for the thinnest slice and ~50% smaller for the thickest. Thus, the influence of

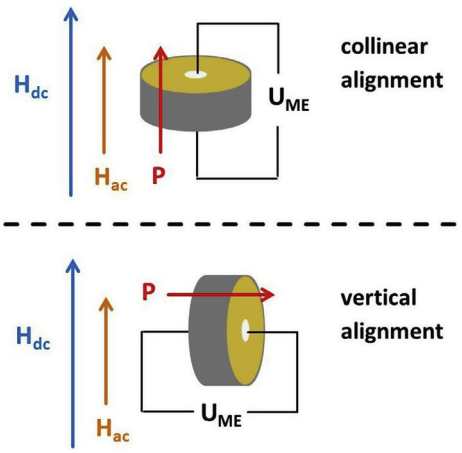

Fig. 10. Scheme of the alignment of electric polarization and magnetic fields for longitudinal and transverse ME measurements.

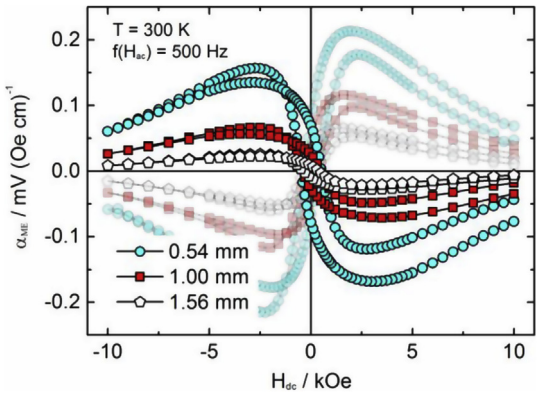

Fig. 11. Field-dependent ME coefficients of the composite $(CoFe_2O_4)_{0.38}$–$(Ba_{0.95}Sr_{0.05}TiO_3)_{0.62}$ grown at 2.5 mm h^{-1}. Transparent symbols correspond to the collinear alignment.

the perpendicular-oriented polarization becomes larger with increasing sample thickness. Agarwal et al. [28] observed a similar behavior (i.e. smaller effect and reversed sign) between a transverse and a longitudinal configuration for bulk composites with a $(BaTiO_3)_{0.6}$–$(CoFe_2O_4)_{0.4}$ stoichiometry, which is close to the eutectic composition. They showed that this characteristic has its origin in the differences between perpendicular and parallel magnetostriction of the samples.

Apart from the opposite sign and reduced magnitude, the ME coefficients follow the same trends for the different sample thicknesses as in the collinear alignment. In addition, the courses of α_{ME} and the position of α_{ME}(max/min) are nearly independent of the alignment in contrast to the bulk composites previously described [28].

4. Conclusions

3-3 heterostructures consisting of 38 mol% $CoFe_2O_4$ and 62 mol% $Ba_{1-x}Sr_xTiO_3$ were synthesized by eutectic crystallization using the floating zone technique. An almost perfect connectivity between the two components was revealed by HR-STEM. Annealing in air at 973 K led to formation of small $BaTiO_3$ inclusions in the $CoFe_2O_4$ phase and a change of $CoFe_2O_4$ orientation near the interface. The epitaxial relationship BTO(001)[100]||CFO(001)[100] was confirmed by single crystal XRD. Samples containing 3 mol% Sr ($CoFe_2O_4$–$Ba_{0.97}Sr_{0.03}TiO_3$) showed an increase of ME coupling from 0.4 to 1.3 mV Oe^{-1} cm^{-1} at room temperature when growth rates were reduced from 20 to 5 mm h^{-1}. Slower crystallization at 2.5 mm h^{-1} resulted in formation of significant amounts of the hexagonal, non-ferroelectric $Ba_{1-x}Sr_xTiO_3$ modification, which was only suppressed by increasing the Sr content to 5 mol%. Unfortunately, this higher Sr content resulted in a strong reduction of α_{ME} due to the smaller electric polarization as reflected by a nearly cubic cell metric. The magnetic DC-field at which the maximum values of α_{ME} occur depended on the sweep direction and a difference in H_{dc}(max) between increasing and decreasing field of 600–700 Oe was observed. Frequency-dependence investigations showed an increase of α_{ME} up to roughly 400 Hz and nearly constant values up to 1000 Hz. In temperature-dependence measurements, local maxima for α_{ME} were found at 260–270 K, reflecting the orthorhombic–tetragonal phase transition of $Ba_{1-x}Sr_xTiO_3$. For thinner samples, an increasing ME coefficient was found. This effect can be rationalized by leakage currents and may explain why thin films have been reported to show much larger ME values. A perpendicular alignment of H and P resulted in a change in sign of the ME coefficient and a 30–50% reduction of the absolute values.

It is striking that the approach of eutectic crystallization has been used rarely since the very first reports in the early 1970s and so far only the $CoFe_2O_4$–$BaTiO_3$ system has been studied. It would be interesting to investigate if this technique can be applied to other multiferroic composite systems as well.

Funding sources

This work was funded by the Deutsche Forschungsgemeinschaft (DFG, German Research Foundation) – project number 31047526 – SFB 762, project A8.

Notes

The authors declare no financial interest.

Acknowledgments

Financial support by the German Research Foundation within the Collaborative Research Centre SFB 762 Functionality of Oxide Interfaces is gratefully acknowledged.

Appendix A. Supplementary data

Supplementary data to this article can be found online at https://doi.org/10.1016/j.jpcs.2019.109076.

References

[1] C.-W. Nan, M.I. Bichurin, S. Dong, D. Viehland, G. Srinivasan, Multiferroic magnetoelectric composites: historical perspective, status, and future directions, J. Appl. Phys. 103 (2008) 031101, , https://doi.org/10.1063/1.2836410.
[2] W. Eerenstein, N.D. Mathur, J.F. Scott, Multiferroic and magnetoelectric materials, Nature 442 (2006) 759–765, https://doi.org/10.1038/nature05023.
[3] D.N. Astrov, Magnetoelectric effect in chromium oxide, Sov. Phys. JETP 13 (1961) 729–733.
[4] M. Etier, V.V. Shvartsman, S. Salamon, Y. Gao, H. Wende, D.C. Lupascu, The direct and the converse magnetoelectric effect in multiferroic cobalt ferrite-barium titanate ceramic composites, J. Am. Ceram. Soc. 99 (2016) 3623–3631, https://doi.org/10.1111/jace.14362.
[5] V.V. Shvartsman, F. Alawneh, P. Borisov, D. Kozodaev, D.C. Lupascu, Converse magnetoelectric effect in $CoFe_2O_4$–$BaTiO_3$ composites with a core–shell structure, Smart Mater. Struct. 20 (2011) 075006, , https://doi.org/10.1088/0964-1726/20/7/075006.
[6] M. Fiebig, Revival of the magnetoelectric effect, J. Phys. Appl. Phys. 38 (2005) R123–R152, https://doi.org/10.1088/0022-3727/38/8/R01.
[7] P.R. Mickel, H. Jeen, P. Kumar, A. Biswas, A.F. Hebard, Proximate transition temperatures amplify linear magnetoelectric coupling in strain-disordered multiferroic $BiMnO_3$, Phys. Rev. B 93 (2016) 134205.
[8] M. Bichurin, V. Petrov, A. Zakharov, D. Kovalenko, S.C. Yang, D. Maurya, V. Bedekar, S. Priya, Magnetoelectric interactions in lead-based and lead-free composites, Materials 4 (2011) 651–702, https://doi.org/10.3390/ma4040651.
[9] A.R. Iordan, M. Airimioaiei, M.N. Palamaru, C. Galassi, A.V. Sandu, C.E. Ciomaga, F. Prihor, L. Mitoseriu, A. Ianculescu, In situ preparation of $CoFe_2O_4$–$Pb(ZrTi)O_3$ multiferroic composites by gel-combustion technique, J. Eur. Ceram. Soc. 29 (2009) 2807–2813, https://doi.org/10.1016/j.jeurceramsoc.2009.03.031.
[10] Y. Liu, Y. Wu, D. Li, Y. Zhang, J. Zhang, J. Yang, A study of structural, ferroelectric, ferromagnetic, dielectric properties of $NiFe_2O_4$–$BaTiO_3$ multiferroic composites, J. Mater. Sci. Mater. Electron. 24 (2013) 1900–1904, https://doi.org/10.1007/s10854-012-1032-y.
[11] M. Etier, V.V. Shvartsman, Y. Gao, J. Landers, H. Wende, D.C. Lupascu, Magnetoelectric effect in (0–3) $CoFe_2O_4$ -$BaTiO_3$ (20/80) composite ceramics prepared by the organosol route, Ferroelectrics 448 (2013) 77–85, https://doi.org/10.1080/00150193.2013.822292.
[12] Y. Liu, Y. Wu, D. Li, Y. Zhang, J. Zhang, J. Yang, A study of structural, ferroelectric, ferromagnetic, dielectric properties of $NiFe_2O_4$–$BaTiO_3$ multiferroic composites, J. Mater. Sci. Mater. Electron. 24 (2012) 1900–1904, https://doi.org/10.1007/s10854-012-1032-y.
[13] T. Walther, U. Straube, R. Köferstein, S.G. Ebbinghaus, Hysteretic magnetoelectric behavior of $CoFe_2O_4$–$BaTiO_3$ composites prepared by reductive sintering and re-oxidation, J. Mater. Chem. C. 4 (2016) 4792–4799, https://doi.org/10.1039/C6TC00995F.
[14] T. Walther, N. Quandt, R. Köferstein, R. Roth, M. Steimecke, S.G. Ebbinghaus, $BaTiO_3$–$CoFe_2O_4$–$BaTiO_3$ trilayer composite thin films prepared by chemical solution deposition, J. Eur. Ceram. Soc. 36 (2016) 559–565, https://doi.org/10.1016/j.jeurceramsoc.2015.10.009.
[15] Y. Shen, J. Sun, L. Li, Y. Yao, C. Zhou, R. Su, Y. Yang, The enhanced magnetodielectric interaction of $(1-x)BaTiO_3$–$xCoFe_2O_4$ multiferroic composites, J. Mater. Chem. C. 2 (2014) 2545, https://doi.org/10.1039/c4tc00008k.
[16] K. Chand Verma, V. Pratap Singh, M. Ram, J. Shah, R.K. Kotnala, Structural, microstructural and magnetic properties of $NiFe_2O_4$, $CoFe_2O_4$ and $MnFe_2O_4$

nanoferrite thin films, J. Magn. Magn. Mater. 323 (2011) 3271–3275, https://doi.org/10.1016/j.jmmm.2011.07.029.
[17] M. George, A. Mary John, S.S. Nair, P.A. Joy, M.R. Anantharaman, Finite size effects on the structural and magnetic properties of sol–gel synthesized $NiFe_2O_4$ powders, J. Magn. Magn. Mater. 302 (2006) 190–195, https://doi.org/10.1016/j.jmmm.2005.08.029.
[18] D. Khomskii, Classifying multiferroics: mechanisms and effects, Physics 2 (2009), https://doi.org/10.1103/Physics.2.20.
[19] N. Quandt, R. Roth, F. Syrowatka, M. Steimecke, S.G. Ebbinghaus, Spin-Coating and characterization of multiferroic MFe_2O_4 (M = Co, Ni)/$BaTiO_3$ bilayers, J. Solid State Chem. 233 (2016) 82–89, https://doi.org/10.1016/j.jssc.2015.10.010.
[20] J. Zhou, H. He, Z. Shi, C.-W. Nan, Magnetoelectric $CoFe_2O_4$/$Pb(Zr_{0.52}Ti_{0.48})O_3$ double-layer thin film prepared by pulsed-laser deposition, Appl. Phys. Lett. 88 (2006) 013111, , https://doi.org/10.1063/1.2162262.
[21] S. Haffer, C. Lüder, T. Walther, R. Köferstein, S.G. Ebbinghaus, M. Tiemann, A synthesis concept for a nanostructured $CoFe_2O_4$/$BaTiO_3$ composite: towards multiferroics, Microporous Mesoporous Mater. 196 (2014) 300–304, https://doi.org/10.1016/j.micromeso.2014.05.023.
[22] M. Breitenbach, S.G. Ebbinghaus, Phase-pure eutectic $CoFe_2O_4$-$Ba_{1-x}Sr_xTiO_3$ composites prepared by floating zone melting, J. Cryst. Growth 483 (2018) 81–88, https://doi.org/10.1016/j.jcrysgro.2017.11.003.
[23] J. Van den Boomgaard, D.R. Terrell, R.A.J. Born, H. Giller, An in situ grown eutectic magnetoelectric composite material, J. Mater. Sci. 9 (1974) 1705–1709.
[24] A. Van Run, D.R. Terrell, J.H. Scholing, An in situ grown eutectic magnetoelectric composite material, J. Mater. Sci. 9 (1974) 1710–1714.
[25] J. Echigoya, Directional solidification and interface structure of $BaTiO_3$-$CoFe_2O_4$ eutectic, J. Mater. Sci. 35 (2000) 5587–5591.
[26] J. Llorca, V. Orera, Directionally solidified eutectic ceramic oxides, Prog. Mater. Sci. 51 (2006) 711–809, https://doi.org/10.1016/j.pmatsci.2005.10.002.
[27] V. Tileli, M. Duchamp, A.-K. Axelsson, M. Valant, R.E. Dunin-Borkowski, N.M. Alford, On stoichiometry and intermixing at the spinel/perovskite interface in $CoFe_2O_4$/$BaTiO_3$ thin films, Nanoscale 7 (2015) 218–224, https://doi.org/10.1039/C4NR04339A.
[28] S. Agarwal, O.F. Caltun, K. Sreenivas, Magneto electric effects in $BaTiO_3$–$CoFe_2O_4$ bulk composites, Solid State Commun. 152 (2012) 1951–1955, https://doi.org/10.1016/j.ssc.2012.08.002.
[29] G.V. Duong, R. Groessinger, Effect of preparation conditions on magnetoelectric properties of $CoFe_2O_4$–$BaTiO_3$ magnetoelectric composites, J. Magn. Magn. Mater. 316 (2007) e624–e627, https://doi.org/10.1016/j.jmmm.2007.03.142.
[30] J. van den Boomgaard, R.A.J. Born, A sintered magnetoelectric composite material $BaTiO_3$-Ni(Co, Mn) Fe_2O_4, J. Mater. Sci. 13 (1978) 1538–1548, https://doi.org/10.1007/BF00553210.
[31] W.P. Wang, H. Yang, T. Xian, R.C. Yu, Observation of abnormal magnetoelectric behavior in 0-3 type $CoFe_2O_4$–$BaTiO_3$ nanocomposites, Chem. Phys. Lett. 618 (2015) 72–77, https://doi.org/10.1016/j.cplett.2014.10.068.
[32] S.Q. Ren, L.Q. Weng, S.-H. Song, F. Li, J.G. Wan, M. Zeng, $BaTiO_3$/$CoFe_2O_4$ particulate composites with large high frequency magnetoelectric response, J. Mater. Sci. 40 (2005) 4375–4378.
[33] E.P. George (Ed.), Materials for Smart Systems: Symposium Held November 28–30, 1994, Materials Research Society, Boston, Massachusetts, U.S.A, 1995Pittsburgh, PA.
[34] H. Ihrig, The phase stability of BaTiO3 as a function of doped 3d elements: an experimental study, J. Phys. C Solid State Phys. 11 (1978) 819.
[35] M. Acosta, N. Novak, V. Rojas, S. Patel, R. Vaish, J. Koruza, G.A. Rossetti, J. Rödel, $BaTiO_3$-based piezoelectrics: fundamentals, current status, and perspectives, Appl. Phys. Rev. 4 (2017) 041305, , https://doi.org/10.1063/1.4990046.
[36] N.J. Ridha, W.M.M. Yunus, S.A. Halim, Z.A. Talib, F.K.M. Al-Asfoor, W.C. Primus, Effect of Sr substitution on structure and thermal diffusivity of $Ba_{1-x}Sr_xTiO_3$ ceramic, Am. J. Eng. Appl. Sci. 2 (2009) 661–664.
[37] R.T. Shannon, Revised effective ionic radii and systematic studies of interatomic distances in halides and chalcogenides, Acta Crystallogr. A. 32 (1976) 751–767.
[38] Y. Tan, J. Zhang, Y. Wu, C. Wang, V. Koval, B. Shi, H. Ye, R. McKinnon, G. Viola, H. Yan, Unfolding grain size effects in barium titanate ferroelectric ceramics, Sci. Rep. 5 (2015), https://doi.org/10.1038/srep09953.
[39] M. Sindhu, N. Ahlawat, S. Sanghi, R. Kumari, A. Agarwal, Crystal structure refinement and investigation of electrically heterogeneous microstructure of single phased Sr substituted $BaTiO_3$ ceramics, J. Alloy. Comp. 575 (2013) 109–114, https://doi.org/10.1016/j.jallcom.2013.04.026.